



HAL
open science

The M, E, and N structural proteins of the severe acute respiratory syndrome coronavirus are required for efficient assembly, trafficking, and release of virus-like particles.

Y. L. Siu, K. T. Teoh, J. Lo, C. M. Chan, F. Kien, N. Escriou, S. W. Tsao, J. M. Nicholls, R. Altmeyer, J. S. M. Peiris, et al.

► **To cite this version:**

Y. L. Siu, K. T. Teoh, J. Lo, C. M. Chan, F. Kien, et al.. The M, E, and N structural proteins of the severe acute respiratory syndrome coronavirus are required for efficient assembly, trafficking, and release of virus-like particles.. *Journal of Virology*, 2008, 82 (22), pp.11318-30. 10.1128/JVI.01052-08 . pasteur-00543224

HAL Id: pasteur-00543224

<https://riip.hal.science/pasteur-00543224>

Submitted on 6 Dec 2010

HAL is a multi-disciplinary open access archive for the deposit and dissemination of scientific research documents, whether they are published or not. The documents may come from teaching and research institutions in France or abroad, or from public or private research centers.

L'archive ouverte pluridisciplinaire **HAL**, est destinée au dépôt et à la diffusion de documents scientifiques de niveau recherche, publiés ou non, émanant des établissements d'enseignement et de recherche français ou étrangers, des laboratoires publics ou privés.

1
2
3
4
5
6
7
8
9
10
11
12
13
14
15
16
17
18
19
20
21
22
23
24
25

The M, E and N structural proteins of the SARS coronavirus are required for efficient assembly, trafficking and release of virus-like particles.

Siu YL.¹, Teoh KT.¹, Lo J.², Chan CM.³, Kien F.¹, Escriou N.⁴, Tsao SW.⁵, Nicholls JM.², Altmeyer R.⁶, Peiris JS.^{1,3}, Bruzzone R.¹ and Nal B.^{1,7}

From the ¹ HKU-Pasteur Research Centre, 8 Sassoon Road, Hong Kong SAR, China; ² Department of Pathology, The University of Hong Kong, Queen Mary Hospital, Hong Kong SAR, China; ³ Department of Microbiology, The University of Hong Kong, 21 Sassoon Road, Hong Kong SAR, China; ⁴ Institut Pasteur, Unité de Génétique Moléculaire des Virus Respiratoires, URA-CNRS 3015, 25-28 Rue du Docteur Roux, 75724, Paris Cedex 15, France; ⁵ Department of Anatomy; The University of Hong Kong, 21 Sassoon Road, Hong Kong SAR, China; ⁶ CombinatoRx-Singapore Pte Ltd, 11 Biopolis Way, 138667 Singapore.

⁷ To whom correspondence should be addressed: e-mail: bnal@hku.hk

Tel: (852)-2816-8403 / Fax: (852)-2872-5782

26 **Abstract**

27

28 Production of virus-like particles (VLPs) constitutes a relevant and safe model to
29 study molecular determinants of virion egress. The minimal requirement for
30 assembly of VLPs for the coronavirus responsible for severe acute respiratory
31 syndrome in humans (SARS-CoV) is still controversial. Recent studies have
32 described that SARS-CoV VLP formation depends on either M and E or M and N
33 proteins. Here we show that both E and N must be co-expressed with M for
34 efficient production and release of VLPs by transfected Vero E6 cells. This result
35 suggests that the mechanism of SARS-CoV assembly differs from other studied
36 coronaviruses, which only require M and E for VLP formation. When co-
37 expressed, the native envelope trimeric S glycoprotein is incorporated onto VLPs.
38 Interestingly, when a fluorescent protein tag is added to the C-terminal end of N or
39 S, but not M, the chimeric viral proteins can be assembled within VLPs and allow
40 visualization of VLP production and trafficking in living cells by state of the art
41 imaging technologies. Fluorescent VLPs will be used further to investigate the role
42 of cellular machineries during SARS-CoV egress.

43

44

45

46

47 **Keywords:** SARS coronavirus, virus-like particle, virus assembly, virus budding,
48 egress, fluorescent viral particles

49

Introduction

50

51

52 Coronaviruses are positive-sense RNA enveloped viruses that belong to the
53 *Coronaviridae* family in the Nidovirales order. These viruses are found in a wide
54 variety of animals and can cause respiratory and enteric disorders of diverse
55 severity (15, 18). In the past five years, several human and animal coronaviruses
56 have been discovered, including the highly pathogenic virus responsible for the
57 severe acute respiratory syndrome (SARS-CoV) (34, 58, 60, 64, 68, 69).
58 Coronavirus particles consist of a helical nucleocapsid structure, formed by the
59 association between nucleocapsid (N) phosphoproteins and the viral genomic
60 RNA, which is surrounded by a lipid bilayer where three or four types of structural
61 proteins are inserted: the spike (S), the membrane (M), the envelope (E) proteins
62 and, for some coronaviruses only, the hemagglutinin-esterase (HE) protein (see
63 for review: (12). Once sufficient amounts of new genomic RNA and structural
64 proteins have been produced, assembly of particles occurs. Assembly and release
65 of virions are the last stages of the virus life cycle.

66 The triple spanning membrane glycoprotein M drives assembly of coronavirus,
67 which bud into the lumen of the endoplasmic reticulum-Golgi intermediary
68 compartment (ERGIC) (32, 33, 62, 63). M is the most abundant envelope protein
69 that sorts viral components to be incorporated into virions. M oligomerisation,
70 mainly driven by its transmembrane domain, is believed to allow formation of a
71 lattice of M proteins at ERGIC membranes (14, 41). S and E membrane proteins
72 are integrated into the lattice through lateral interactions with M, whereas N and
73 viral RNA interact with M C-terminal domain, which is exposed to the cytosol (4, 8,
74 13, 19, 30, 36, 48, 54, 55). The coronavirus S protein, responsible for receptor

75 binding and membrane fusion, does not seem to have any major role in
76 coronavirus assembly. Recent studies show that E is a viroporin that forms ion
77 channels (46, 66, 67). Despite its minor incorporation into virion particles (7, 22,
78 40), the small E protein plays an important but not fully understood role in virus
79 morphogenesis and budding (20, 35, 70). Studies performed on coronaviruses,
80 including the SARS-CoV, demonstrate that depletion of the E gene from
81 coronavirus genome strongly diminish virus growth and particle formation (9, 16,
82 35, 37, 57). The N protein self-associates and encapsidates the RNA genome for
83 incorporation into budding virions through interactions with the M protein
84 independently of E and S proteins (24, 52, 53, 61). For SARS-CoV, the interaction
85 of N with M was described to be independent of viral RNA (25, 45).

86 Work on mouse hepatitis virus (MHV), bovine coronavirus (BcoV), infectious
87 bronchitis virus (IBV) and transmissible gastroenteritis virus (TGEV) has
88 established that E and M proteins are necessary and sufficient for assembly of
89 virus-like particles (VLPs), which share size and morphological features with real
90 viruses (1, 2, 7, 8, 38, 65). Nevertheless, the minimal requirement for assembly of
91 SARS-CoV VLPs is still controversial. Huang Y. and colleagues described
92 formation of VLPs in transfected human 293 renal epithelial cells that only required
93 co-expression of the M and N viral proteins (29). On the contrary, other studies
94 described that co-expressed M and E proteins were sufficient for release of
95 sedimentable particles from transfected mammalian cells (27) or insect cells, using
96 a baculovirus expression system (26, 50). A few groups have proposed
97 immunization with SARS-CoV VLPs as an effective vaccine strategy. VLPs
98 produced in insect cells or chimeric MHV/SARS-CoV VLPs produced in
99 mammalian cells were used in these studies (42, 44).

100 Our objective was to delineate the molecular mechanisms that regulate SARS-
101 CoV egress in mammalian cells. Here we demonstrate that whereas VLPs could
102 hardly be recovered from culture medium of cells co-expressing combinations of M
103 and E or M and N proteins, co-expression of both SARS-CoV E and N with M
104 allowed release of significant levels of VLPs within one day. When co-expressed,
105 the trimeric S protein was found in VLPs. Therefore, in apparent contrast to other
106 coronaviruses, SARS-CoV egress strongly depends on three structural proteins:
107 M, E and N. Addition of fluorescent tags to viral structural proteins allowed us to
108 visualize egress of fluorescent VLPs in living cells. Monitoring of VLPs egress in
109 living cells will be a powerful new tool to study the involvement of viral and cellular
110 factors during the late stages of the SARS-CoV life cycle.

111

Materials and Methods

112

113

114 **Cells and culture conditions.** The Vero E6 African Green Monkey kidney cell line
115 was cultured in Dulbecco's modified Eagle's medium supplemented with 10%
116 heat-inactivated foetal calf serum, 100 U of penicillin and 100 µg of streptomycin
117 per ml, at 37°C with 5% CO₂.

118

119 **Plasmid constructions.** CDNAs coding for the SARS-CoV M, E, S and N
120 structural proteins were codon-optimized for mammalian cells and synthesized by
121 GeneArt (Regensburg, Germany). The M cDNA was amplified by PCR and sub-
122 cloned into the pIRES plasmid vector (BD Biosciences, San Jose, CA, USA)
123 between the Nhe I and EcoR I restriction sites of the upstream multiple cloning
124 site. The E cDNA was amplified by PCR and inserted either into the pcDNA3.1
125 plasmid vector between the Kpn I and Not I restriction sites or into the pIRES
126 plasmid vector between the Sal I and Not I restriction sites of the downstream
127 multiple cloning site. The S cDNA was amplified by PCR and inserted either into
128 the pcDNA3.1 plasmid vector between the Nhe I and Apa I restriction sites. The
129 pcDNA-Nflag plasmid was constructed from the original pCRScript-Nflag
130 (produced by GeneArt, Regensburg, Germany) using the Kpn I and Xho I
131 restriction sites. The Flag tag was in fusion with the 3' end of N cDNA and
132 separated from N cDNA by six nucleotides encoding two glycine residues. The
133 cDNAs coding for the enhanced yellow (eYFP), cyan (eCFP), green (eGFP)
134 fluorescent proteins and the monomeric red fluorescent protein (mRFP1, (5), were
135 amplified by PCR from plasmids purchased from Clontech Laboratories (Takara
136 Bio, Shiga, Japan) and subcloned into pcDNA3.1 or pIRES vectors. Then S, N or

137 M cDNAs were inserted in 5' of the fluorescent protein cDNAs using Cla I and Apa
138 I sites (S and N) or Xho I and Mlu I (M) restriction sites. The two fused cDNAs
139 were separated by two codons encoding glycines.

140

141 **Antibodies.** The M and E proteins were detected with rabbit polyclonal antibodies
142 raised against the C-terminal extremity of each protein. The rabbit polyclonal
143 antibody against the M C-terminal domain was purchased from ProSci
144 Incorporated (Poway, CA, USA). The rabbit polyclonal antibody against the E
145 protein was produced by Dr Nicolas Escriou (Institut Pasteur, Paris) using a C-
146 terminal peptide. The Flag tag was detected with the mouse monoclonal IgG1 M2
147 antibody purchased from Sigma-Aldrich. The mouse polyclonal antibody against
148 the S protein was obtained by immunizing mice with purified S trimers expressed
149 in mammalian cells as described previously (31). The mouse monoclonal antibody
150 against the N protein was a generous gift from Dr Chan KH (Department of
151 Microbiology, the University of Hong Kong) and produced as described in (56).

152

153 **Transient transfections and production of SARS-CoV VLPs.** Eight hundred
154 thousand cells were plated in 75 cm² dishes, incubated over-night and transfected
155 with plasmid constructs using the FuGENE 6 transfection reagent (Roche, Basel,
156 Switzerland), according to the manufacturer's instructions. Briefly, 54 µl of
157 FuGENE 6 transfection reagent were mixed with DMEM, incubated for five
158 minutes and then 6 µg of each plasmid were added. The FuGENE 6 / plasmid
159 mixture was incubated for 30 minutes at room temperature. Cell medium was
160 discarded and replaced with 3 ml of warm DMEM. The FuGENE 6 / plasmid
161 mixture was added to the cells. After 3 hours of incubation at 37°C, the medium

162 containing the transfection mixture was discarded and 10 ml of fresh medium was
163 added. Cells were incubated for 21 or 45 hours.

164

165 **Purification of SARS-CoV VLPs.** At 24 or 48 hours post-transfection, cell
166 medium was collected and cleared by centrifugation at low speed (1000g for 10
167 minutes) to pull-down cell debris. After passing through 0.45 μm filter, cleared cell
168 medium were then loaded on top of 20% sucrose cushions and ultra-centrifuged
169 for 3 hours at 28,000 rpm using a SW41 rotor (Beckman Coulter Inc, Fullerton, CA,
170 USA). VLP-containing pellets were resuspended in Tris HCl 50 mM NaCl 100 mM
171 EDTA 0.5 mM pH7.4 (TNE) buffer.

172

173 **Western blot analysis of VLPs and cell lysates.** For Western blot analysis of
174 purified VLPs, 15 μl of resuspended pellets from ultracentrifuged culture medium
175 were mixed with 5 μl lithium dodecyl sulfate (LDS)-containing loading buffer and
176 loaded on 4 to 12 % polyacrylamide gels (NuPAGE Novex Bis-Tris Mini Gels,
177 Invitrogen, Carlsbad, CA, USA). Electrophoresis was performed with the NuPAGE
178 MOPS SDS Running Buffer from the same manufacturer. Alternatively,
179 resuspended pellets from 48 hours time points were loaded on top of 20 to 60%
180 sucrose gradients and ultracentrifuged for 3.5 hours at 26,700 rpm (27). Twenty
181 fractions were collected and analyzed by Western blot. For Western blot analysis
182 of cell lysates, cells were washed twice with PBS 1X at 24 or 48 hours post-
183 transfection, and lysed in lysis buffer containing 1% Triton X-100, 150 mM NaCl,
184 20 mM Tris-HCl pH7.5 and 1 mM EDTA for 15 minutes on ice with frequent
185 vortexing. Then lysates were cleared by centrifugation at 16100 g for 15 minutes
186 at 4°C and analyzed by Western blot. 15 μl of each lysate were mixed with 5 μl

187 LDS loading buffer and loaded on polyacrylamide gels. For detection of E but S,
188 samples were treated with dithiothreitol and heated at 95°C for 5 minutes before
189 migration on polyacrylamide gels. To detect both E and trimers of S from same
190 preparations, samples were split and either treated or not before loading of two
191 separate gels for E and S detection, respectively. Results for M and Nflag were
192 similar with or without treatment.

193

194 **Electron microscopy.** For transmission electron microscopy experiments,
195 transfected cells were harvested at 24 and 48 hours post-transfection. Cells were
196 detached using 10 mM EDTA, fixed in 2.5 % glutaraldehyde in cacodylate buffer
197 and post-fixed with 1% Osmium Tetroxide (OsO₄) in Cacodylate buffer for 1 hour
198 at room temperature. Then cells were embedded in 2% agarose to form cell blocks
199 which were then dehydrated in graded series of ethanol and embedded in epoxy
200 resin. Ultrathin sections were stained for 45 minutes with 2% aqueous uranyl
201 acetate and for 30 minutes with Reynolds' lead citrate. For analysis of secreted
202 VLPs, VLPs were purified from cell medium by ultracentrifugation on 20% sucrose
203 cushion, separated on 20-60% discontinuous sucrose gradient and fraction 10 was
204 collected and then concentrated by ultracentrifugation in TNE buffer, pH 7.4 for
205 one hour at 28,000 rpm. 5µl of the VLP suspension, mixed with equal volume of
206 negative stain (2% aqueous uranyl acetate and 2% phosphotungstate solution, pH
207 7.0), was placed onto a formvar-carbon-coated copper grid for 2 minutes, excess
208 suspension were drained. The grids were viewed and photographed with a Philip
209 CM100 electron microscope at 80 kV.

210

211 **Fluorescence microscopy.** For fluorescence microscopy on fixed cells, Vero E6
212 cells were grown on glass coverslips, transfected and analyzed at 24 hours post-
213 transfection. Cells were washed with PBS, nuclei were stained with DAPI and
214 coverslips were mounted on glass slides for analysis. Fixed cells were visualized
215 under AxioObserver Z1 inverted motorized fluorescent microscope using the
216 ApoTome module and piloted through the Axiovision 4.6 software and images
217 were acquired through the MRm AxioCam high resolution CCD camera (Carl
218 Zeiss, Germany). For fluorescence microscopy on live cells, Vero E6 cells were
219 grown in glass-bottom culture dish (MatTech, USA), transfected and analyzed at
220 24 hours post-transfection. Cells were washed and medium was changed to
221 HBSS, Optimem pre-warmed culture medium. Widefield image acquisitions of live
222 cells were obtained using the system described above. Confocal acquisitions of
223 live cells were acquired at the Hong Kong University Core Imaging Facility using
224 an AxioObserver Z1 inverted motorized fluorescent microscope equipped with a
225 spinning disc confocal imaging system (UltraVIEW ERS, PerkinElmer, Shelton,
226 CT, USA). For brefeldin A (BFA) treatment, cells were incubated with 6 μ g per ml
227 of BFA for indicated times. To release BFA effect, cells were washed three times
228 in PBS 1X and reincubated in normal medium for indicated times.
229

Results

230

231

232 **Efficient production and release of SARS-CoV VLPs are driven by co-**
233 **expression of M, N and E structural proteins.**

234 To determine the optimal conditions for efficient SARS-CoV VLP production, we
235 chose to co-express different combinations of structural proteins in the Vero E6
236 African green monkey cell line, which is permissive to SARS-CoV replication (34).
237 cDNAs encoding SARS-CoV structural proteins M, E and N were codon-optimized
238 for expression in mammalian cells. Understanding the importance to maintain a
239 low E/M ratio in transfected cells to ensure concomitant expression of E and M,
240 low incorporation of E into VLPs and prevent potential formation of E-containing
241 vesicles, we reasoned that the use of the pIRES bi-cistronic plasmid should be
242 appropriate. This plasmid presents the double advantage to ensure co-expression
243 of both cDNAs in transfected cell and allows a reduced rate of translation of the
244 downstream gene by utilizing a partially disabled internal ribosome entry site
245 (IRES) sequence. We therefore subcloned M upstream of E cDNA in the pIRES
246 vector. N was expressed from a pcDNA plasmid with a C-terminal Flag tag. Vero
247 E6 cells were either not transfected or transfected with pcDNA-E, pIRES-M or
248 pIRES-M-E alone, pIRES-M plus pcDNA-Nflag and pIRES-M-E plus pcDNA-Nflag
249 (Figure 1A). At 24 and 48 hours post-transfection culture medium and cells were
250 harvested. Culture medium was subjected to ultracentrifugation on a 20% sucrose
251 cushion to isolate VLPs and the SARS-CoV structural proteins assembled into
252 VLPs were analyzed by Western blot.

253 The M protein was readily detected at both 24 and 48 hours post-transfection in
254 lysates from Vero E6 cells transfected with pIRES-M, pIRES-M-E, pIRES-M plus

255 pcDNA-Nflag and pIRES-M-E plus pcDNA-Nflag (Figure 1A, upper panels). As
256 described previously, three major forms of M, which correspond to different
257 glycoforms, were detected on SDS-PAGE: two bands at ~ 18 and 28 KDa and a
258 smear at higher molecular sizes reflecting heterogeneity of glycosylation patterns
259 (51). As expected, higher levels of M were detected in cell lysates at 48 hours than
260 at 24 hours post-transfection. Whereas a 10 KDa protein corresponding to E could
261 be easily detected in cell lysates from cells transfected with pcDNA-E plasmid, its
262 expression was much lower in cells transfected with the pIRES-M-E bi-cistronic
263 vector. The Nflag protein was found in cell lysates from both pIRES-M plus
264 pcDNA-Nflag and pIRES-M-E plus pcDNA-Nflag transfected cells at similar levels.
265 A major band corresponding to a protein with an apparent molecular size of 45
266 KDa was detected.
267 Strikingly, the efficacy of VLP production was dramatically affected by the
268 combination of viral proteins co-expressed (Figure 1A, lower panels). Although M
269 was not detected in ultracentrifuged culture medium from pIRES-M, pIRES-M-E or
270 pIRES-M plus pcDNA-Nflag transfected cells at 24 hours post-transfection,
271 significant levels were found in preparations from pIRES-M-E plus pcDNA-Nflag
272 transfected cells. Similarly, the N protein was only detected in ultracentrifuged
273 culture medium from pIRES-M-E plus pcDNA-Nflag transfected cells at this early
274 time point. Signals for E were below the limit of detection at 24 hours and
275 detectable only at 48 hours. Finding low amounts of E in VLPs is in accordance
276 with the minor presence of this protein in coronavirus particles, despite its
277 important role for virion assembly and budding (9, 20, 37, 57, 65). In conclusion,
278 only when M, E and N proteins were co-expressed, VLPs that contained the M and
279 N proteins could be isolated from culture medium at 24 hours post-transfection.

280 At 48 hours post-transfection, E was found in ultracentrifuged culture medium from
281 cells transfected with the pcDNA-E plasmid alone. This is in agreement with
282 previously published data that describe secretion of E proteins independently of
283 other viral elements (7, 47, 50). At this time point, trace amounts of M were
284 detected in ultracentrifuged culture medium from pIRES-M and pIRES-M-E
285 transfected cells, whereas significant levels of M and N were found for pIRES-M
286 plus pcDNA-Nflag ultracentrifuged culture medium. Independent secretion of
287 SARS-CoV M proteins from Vero E6 cells as well as production of M-E VLPs was
288 described by Mortola and Roy (2004) at four days post-transfection. Production of
289 SARS-CoV M-N VLPs has already been reported by Huang Y. and colleagues in
290 transfected 293 renal epithelial cells at 63 hours post-transfection (29). Very
291 interestingly, in our conditions, significantly higher levels of M and N proteins were
292 found in purified VLPs from pIRES-M-E plus pcDNA-Nflag than pIRES-M plus
293 pcDNA-Nflag transfected cells at 48 hours post-transfection. We were also able to
294 detect E in these conditions, but not when cells were only transfected with the
295 pIRES-M-E vector.

296 In order to verify that inefficacy of production of M-E VLPs by cells transfected with
297 pIRES-M-E was not due to inefficient E expression, we performed similar
298 experiments but expressed E from a pCDNA-E plasmid and analyzed cells and
299 medium at 48 hours post-transfection (Figure 1B). As expected, higher levels of E
300 were detected in lysates of cells transfected with pIRES-M plus pCDNA-E and
301 pIRES-M plus pCDNA-E plus pCDNA-Nflag than pIRES-M-E and pIRES-M-E plus
302 pCDNA-Nflag, respectively (Figure 1B, left panel). Nevertheless, neither
303 production of M-E VLPs nor M-E-N VLPs were improved by increase of E
304 expression (Figure 1B, right panel). On the contrary, production of M-E-N VLPs

305 was enhanced when the bicistronic vector was used, as indicated by higher levels
306 of Nflag, M and E proteins secreted, and the ratio E(medium)/E(lysate) was
307 significantly higher in these conditions. This result suggests that expression of E
308 along with M from the pIRES-M-E bicistronic vector and in combination with N is
309 favorable to the production of SARS-CoV VLPs.

310 We then investigated co-sedimentation of secreted viral structural proteins by
311 performing sucrose gradient fractionation on ultracentrifuged cell medium. Cells
312 were either transfected by individual plasmids or combinations of plasmids as
313 described previously. In this experiment we used the individual plasmid for E
314 expression to verify potential presence of E-containing vesicles in medium when E
315 was expressed at higher levels. At 48 hours post-transfection, cleared cell medium
316 was ultracentrifuged on 20% sucrose cushion and pellets were resuspended in
317 TNE buffer. As controls, viral proteins contained in cell lysates and pellets from
318 ultracentrifuged medium were analyzed by Western blot (Figure 1C, left panel).
319 Pellets were loaded on top of 20-60% discontinuous sucrose gradients. After
320 another round of ultracentrifugation, 20 fractions were collected and analyzed by
321 Western blot (Figure 1C, right panels a to e). Results were consistent with the data
322 described in Figure 1 A and B. When M was expressed alone, very little amounts
323 of protein were found in cell medium and traces were detected in fraction 9 (Figure
324 1C, panel a). Coexpression with E or Nflag, allowed secretion of slightly higher
325 levels of M in cell medium and detection of M in fractions 7 to 11, with enrichment
326 in fraction 10 (Figure 1C, panel c) or 11 (Figure 1C, panel d), respectively. E
327 protein was not detectable in fractions from medium of either pCDNA-E or pIRES-
328 M plus pCDNA-E transfected cells (Figure 1C, panel b and c). Nflag cosedimented
329 with M when co-expressed (Figure 1C, panel d). As expected, greater levels of M,

330 E and Nflag proteins were found in medium of cells expressing all three viral
331 proteins (Figure 1C, panel e). M and Nflag were present in fractions 5 to 14 with
332 proportional levels. E was detected in fractions 8 to 10 where M and N proteins
333 were also enriched. Altogether, these results show that secreted viral structural
334 proteins cosediment in sucrose gradient and therefore strongly suggest that viral
335 proteins are associated into VLPs. Moreover, secretion of E-containing vesicles
336 does not seem to be a major phenomenon in Vero E6 cells expressing E alone or
337 in combination with other viral proteins in our system. Indeed, in all conditions,
338 levels of E in cell medium were systematically low and only detected in fractions
339 when co-expressed with M and N.

340 Altogether these data establish for the first time that all three M, E and N structural
341 SARS-CoV proteins are important for efficient production and release of SARS-
342 CoV VLPs.

343

344 **S is incorporated onto SARS-CoV M-E-N-containing VLPs.**

345 We then investigated whether the SARS-CoV S glycoprotein could be
346 incorporated onto secreted M-E-N VLPs. S cDNA was codon optimized and
347 subcloned in the pcDNA vector. Vero E6 cells were transfected with pIRES-M-E
348 plus pcDNA-Nflag plus pcDNA-S. Protein expression was verified in cell lysates at
349 48 hours post-transfection (data not shown). To monitor association of S onto M-
350 E-N VLPs, we performed sucrose fractionation on VLPs previously purified from
351 culture medium (Figure 2). All S, Nflag, M and E proteins were co-sedimented and
352 enriched in fractions 9 and 10 corresponding to ~40% sucrose. It is notable that S
353 was mainly detected in its native trimeric form in these fractions (540 KDa),
354 although we also detected low levels of monomers (180 KDa) and dimers (360

355 kDa), which may have resulted from sample treatment and SDS-PAGE conditions.
356 Higher molecular weight proteins, detected with anti-S antibodies, were found in
357 the lightest fractions 1 to 6. These forms could correspond to soluble, non-
358 incorporated forms of S proteins that have formed aggregates. We have previously
359 described formation of S aggregates in preparations of purified SARS-CoV S
360 trimers from mammalian cell lysates (31). This result confirms association of all
361 four SARS-CoV structural proteins into S-M-E-N VLPs that can be purified from
362 culture medium of transfected cells.

363

364 **VLPs bud into a perinuclear compartment and are transported within**
365 **vesicles to the plasma membrane.**

366 We next studied the subcellular localization of SARS-CoV VLPs by electron
367 microscopy (Figure 3). pIRES-M-E plus pcDNA-Nflag plus pcDNA-S co-
368 transfected Vero E6 cells were fixed at 24 and 48h post-transfection and ultrathin
369 sections were prepared for transmission electron microscopy (Figure 3A to G).
370 Large amounts of VLPs, with diameters ranging from 40 to 150 nm on sections,
371 were found within the cytoplasm of positive cells. Three main patterns of
372 subcellular localization were observed. First, VLPs were found within perinuclear
373 compartments, which had appearance of groups of vacuoles (Figure 3A, C and D),
374 or, alternatively but seldom observed, which presented morphological
375 characteristics of the endoplasmic reticulum (Figure 3B). Vacuoles were observed
376 at both 24 hours and 48 hours post-transfection with a diameter ranging from 300
377 nm to 1.5 μ m on sections. Very interestingly, we detected several events of VLP
378 budding at vacuole membranes (Figure 3D). Although VLPs accumulated therein,
379 they were not highly compacted in this compartment. Moreover, VLPs appeared

380 pleiomorphic and heterogenous material was also observed (Figure 3D). Tubular
381 structures were seen within some VLP-containing vacuoles, mainly at 24 hours
382 post transfection (data not shown). Second, VLPs were observed in vesicles
383 scattered in the cytoplasm (Figure 3A, B, C and E). These vesicles had a diameter
384 ranging from 200 nm to 1 μ m on sections and VLPs were more compacted inside.
385 They could be found at proximity of the perinuclear VLP-containing compartments
386 up to the cortical area. VLPs contained in these vesicles looked more
387 homogenous in size and shape. Third, VLPs were occasionally found at the cell
388 surface (Figure 3A, F and G). Although we could not observe obvious spike-like
389 structures surrounding the VLP envelope, spike-like protuberances were
390 occasionally detected (Figure 3G). Moreover, binding of VLPs to cell surface
391 suggests the presence of spikes and receptor recognition. Some cells, in which
392 very high amounts of VLPs were found, presented characteristics of apoptosis with
393 fragmented nucleus and disrupted membranes (data not shown). The cytoplasm of
394 these cells was filled up with VLPs, either free or within intracellular compartments.
395 The morphology of released VLPs was investigated further by electron microscopy
396 on negatively stained particles that were purified from cell medium (Figure 3F).
397 Round-shaped particles with a diameter of 80-100 nm were readily observed.
398 Again, we could not observe the typical corona of spikes around VLPs (21) but
399 globular structures protruding from VLPs were detected, which likely corresponded
400 to trimers of spikes. Altogether, our data suggest that SARS-CoV VLPs bud in an
401 intracellular compartment of Vero E6 cells and are efficiently transported within
402 vesicles to the plasma membrane where they are released. Shape and size of
403 secreted VLPs are in accordance with the morphological characteristics of the

404 SARS-CoV and therefore these VLPs should be a safe and appropriate model to
405 study assembly and release of SARS-CoV virions.

406

407 **Assembly and release of VLPs that incorporate fluorescently-tagged**
408 **structural viral proteins.**

409 In order to visualize in real time, the assembly, trafficking and release of SARS-
410 CoV VLPs, we engineered plasmid constructs that allow expression of viral
411 proteins in fusion with fluorescent proteins. The pIRES-MmRFP1-E, pcDNA-
412 NeCFP and pcDNA-SeYFP constructs were developed and expression of fusion
413 viral proteins was analyzed in individually transfected or co-transfected cells by
414 fluorescence microscopy (Figure 4). We did not include any construct coding for a
415 fluorescently tagged SARS-CoV E protein because it does not tolerate fluorescent
416 protein tags (C. Chan et al., unpublished data). All chimeric viral proteins could be
417 readily observed by fluorescent microscopy. In cells individually transfected with
418 the pIRES-MmRFP1-E, the MmRFP1 fusion protein was mainly present in a
419 perinuclear compartment, most likely the ERGIC/Golgi apparatus (Figure 4, panels
420 a,b). We also found MmRFP1 within the cytoplasm and occasionally at the plasma
421 membrane. As expected, the SeYFP protein was observed both in the
422 ERGIC/Golgi apparatus, and at the plasma membrane of individually transfected
423 cells (Figure 4, panels c,d). These expression patterns are similar to what we
424 observed previously for MeGFP and SeGFP fusion proteins at 15 hours post-
425 infection with Semliki Forest Virus expression vectors (51). In most of the cells,
426 individually expressed NeCFP protein formed bright cytosolic patches, suggesting
427 aggregation of the protein in the cytosol in absence of functional viral protein
428 partners (Figure 4 e,f). This pattern may reflect large inclusions of nucleocapsids,

429 which have been described to accumulate late in the infection of cells with HCoV
430 and MHV-JHM and SARS-CoV (6, 17, 23) or may constitute a cytosolic reservoir
431 of protein supposed to feed the viral budding system. Interestingly, when plasmids
432 were co-transfected, all three MmRFP1, SeYFP and NeCFP fluorescent proteins
433 presented similar intracellular distributions, co-localizing in the cytoplasm and at
434 the plasma membrane (Figure 4 panels g,i,k,m and h,j,l,n). When co-expressed
435 with MmRFP1, E and SeYFP, the subcellular distribution of the NeCFP protein
436 was dramatically changed and bright cytosolic patches were rarely found (Figure
437 4, panels e,f and k,l). Trafficking of NeCFP to the cell surface in co-transfected
438 cells suggests that interactions with other viral proteins have occurred leading to
439 NeCFP translocation. Nevertheless no VLPs were detected in medium from co-
440 transfected cells (data not shown). Altogether, these results suggest that although
441 MmRFP1, SeYFP, NeCFP and E are likely to interact when co-expressed in Vero
442 E6 cells, they are not released in the form of VLPs in cell medium.

443 We then reasoned that fluorescent VLPs could be produced by including only one
444 plasmid coding for one of the fluorescently tagged viral protein per co-transfection.
445 In these conditions, we investigated protein expression and release of VLPs by
446 Vero E6 cells at 48 hours post-transfection (Figure 5A). As positive control, we
447 monitored VLP release from pIRES-M-E, pcDNA-Nflag, pcDNA-S transfected
448 cells. As expected, S, Nflag, M and E proteins were detected in both cell lysate
449 and VLP preparation (Figure 5A, lane 2 and 7). Although the MmRFP1 fusion
450 protein was readily observed by fluorescent microscopy, it could not be detected
451 by Western blot. Most likely, the rabbit polyclonal antibody directed against the M
452 C-terminal domain cannot recognize its epitope when it is fused to the mRFP1
453 fluorescent tag. Although the E, Nflag and S proteins were detected on cell lysate

454 from pIRES-MmRFP1-E plus pcDNA-Nflag plus pcDNA-S transfected cells (Figure
455 5A, lane 3), no protein corresponding to purified VLPs were found in medium
456 (Figure 5A, lane 8). We concluded that fusion of the mRFP1 protein at the C-
457 terminal end of M inhibits VLP production. On the contrary, both pIRES-M-E plus
458 pcDNA-NeCFP plus pcDNA-S, as well as pIRES-M-E plus pcDNA-Nflag plus
459 pcDNA-SeYFP transfected cells were able to release VLPs in cell medium, as
460 indicated by the presence of viral proteins (figure 5A, lanes 9 and 10). Under these
461 conditions, the NeCFP protein was detected by a mouse monoclonal antibody
462 directed against N (56) and migrated to an apparent molecular size of 70 KDa.
463 To confirm that NeCFP or SeYFP viral proteins are correctly incorporated into
464 VLPs, we analyzed purified VLPs by fractionation on a 20-60% sucrose gradient
465 (Figure 5B). Both NeCFP and SeYFP co-sedimented with other viral proteins,
466 indicating that they were incorporated in purified VLPs (Figure 5B, upper and lower
467 panels, respectively). M-E-NeCFP-S VLPs were concentrated in fractions 10 and
468 11. The E protein was not detected, most likely because M-E-NeCFP-S VLPs
469 were less abundant in culture medium than M-E-Nflag-S VLPs for which E levels
470 were already low. M-E-Nflag-SeYFP VLPs were more efficiently produced and
471 concentrated in fractions 9 and 10 although high levels were also found in
472 fractions 6, 7 and 8. Considering the high levels of M and Nflag detected in these
473 fractions, incorporation of SeYFP seems less efficient than S (cf. Figure 2 with
474 Figure 5B, lower panel). Altogether, our results demonstrate that fluorescent VLPs
475 can be readily produced in Vero E6 transfected cells by incorporating either a
476 tagged N or S fusion protein.
477

478 **Visualization of M-E-NeC/GFP-S VLP production and transport in living Vero**
479 **E6 cells.**

480 We then investigated formation and transport of fluorescent SARS-CoV VLPs in
481 living transfected cells by fluorescent microscopy. Knowing that S is expressed all
482 along the secretory pathway in both single- and co-transfected cells, we reasoned
483 that N would be a better marker for monitoring of SARS-CoV VLPs assembly.
484 Furthermore, having demonstrated that M, E and N are the crucial factors for
485 assembly and egress of SARS-CoV VLPs, and anticipating that S-bearing VLPs
486 could be internalized back into producer cells by ACE-2 driven endocytosis, we
487 decided to omit S. Therefore, the pcDNA-NeCFP plasmid was either transfected
488 alone or co-transfected with pIRES-M-E. Vero E6 cells were analyzed at 24 hours
489 post-transfection. In most pcDNA-NeCFP transfected cells, eCFP signals were
490 very bright and concentrated in large aggregates in the cytosol at the periphery of
491 the nucleus (Figure 6A, panel a). Inversely and very interestingly, a different
492 pattern was observed in most of cells co-transfected with pIRES-M-E and pcDNA-
493 NeCFP. In these cells, eCFP fluorescence was more diffuse in cell cytosol:
494 medium-size bright vesicles were concentrated in close proximity to the nucleus,
495 smaller and dimmer vesicles were scattered in the cytoplasm and occasionally
496 bright dots were enriched at the cell cortical area (Figure 6A, panels b). Few bright
497 dots were also found outside cells in the surrounding medium. This difference in
498 NeCFP distribution pattern, suggests that NeCFP assembles with co-expressed M
499 and E viral proteins to form VLPs and traffics from the perinuclear assembly
500 compartment to the cell surface where fluorescent VLPs are released into the
501 medium.

502 We then further analyzed the trafficking dynamics of a fluorescently tagged N
503 protein, co-expressed with M and E envelope proteins in living Vero E6 cells. In
504 this aim, images were acquired using a spinning disc confocal microscope coupled
505 to a CCD camera suitable for high-speed and high-resolution imaging. In these
506 experiments we replaced the NeCFP by a NeGFP fusion protein, which is
507 excitable by the Argon laser the microscope was equipped with. We could
508 consistently identify three types of NeGFP containing vesicles, where fluorescent
509 signal intensities, sizes and movements differ (Figure 6B and corresponding
510 videos provided as supplementary data). First, the largest and brightest vesicles
511 were found close to the nucleus and were static. Second, smaller and dimmer
512 vesicles were trafficking actively, most of the time in a multidirectional way, making
513 transient interactions with other vesicles. Occasionally these vesicles moved in
514 rapid, unidirectional way and for longer distances, most likely along microtubules.
515 Third, some cells presented an accumulation of bright dots at the cortical area,
516 which may correspond to smaller secretory vesicles and released VLPs. Few
517 bright dots were found outside cells, which probably correspond to fluorescent
518 VLPs that have been released from producer cells. These results illustrate that
519 fusion of a fluorescent tag to the C-terminal end of the nucleocapsid viral protein
520 makes monitoring of SARS-CoV VLPs' egress possible.

521 We then investigated the effect of Brefeldin A (BFA), a fungal metabolite that has
522 multiple effects upon the organelles of the secretory pathway, including inhibition
523 of trafficking from ER to the Golgi apparatus, fusion of the cisternae of the Golgi
524 with the ER and fusion of the trans-Golgi network (TGN) with endosomes (59).
525 BFA has been used in previous study for analysis of viral protein transport and
526 virus assembly (10, 49). Time-lapse images of living Vero E6 cells transfected with

527 M-E plus NeGFP were acquired at 24 hours post-transfection (Figure 6C; for
528 video, see supplementary data). In a first time, cells were either non-treated (panel
529 a) or treated with 6 μg / ml BFA for 4 hours (panel d) or over-night (panel g). After
530 several minutes of acquisition in these conditions, medium was changed to either
531 BFA-containing medium (panels b and c) or normal medium (panels e, f and h, i),
532 respectively. New sequences of images were acquired and fluorescence
533 redistribution was analyzed. Upon BFA treatment we observed fusion of scattered
534 fluorescent vesicles into large cytosolic fluorescent clusters accumulating at the
535 center of the cell and diminution of puncta (panels a, b and c, supplementary
536 data). After treatment of cells for 4 hours with BFA, most of the fluorescence was
537 present in large bright patches surrounding the nucleus (panel d). Vesicles could
538 still be observed in the cytosol, although less numerous than in non-treated cells.
539 Following BFA wash, we could not observe any obvious reversibility of the
540 massive redistribution of fluorescence (compare panels d and e, panel f). After
541 over-night incubation with BFA, fluorescence was associated with large cytosolic
542 clusters and endoplasmic reticulum (panel g) and no drastic change was observed
543 after BFA wash and 1:30 hours recovery (panel h), although membrane dynamics
544 seem to increase at the edge on the reticular compartment where tubules
545 elongated from (panel h, arrow; supplementary data). Three hours recovery after
546 over-night BFA treatment partially restore trafficking of fluorescent vesicles in
547 transfected cells (panel i). The recovery process after BFA treatment was slow and
548 the dynamics could not be followed for several hours, as repetitive exposure to
549 laser induced apoptosis. Altogether, our results suggest 1/ that BFA induce
550 reorganization of NeGFP associated compartments and alters vesicle formation
551 and transport, 2/ that several hours of recovery after BFA wash are necessary to

552 restore dynamics of NeGFP associated compartment and vesicles trafficking.
553 Further studies are required in order to clarify the subcellular compartments VLPs
554 are associated with and delineate the dynamics of egress in association with
555 cellular structures.
556

ACCEPTED

Discussion

557

558

559 The minimal molecular requirement for efficient assembly and egress of SARS-
560 CoV virions is still controversial. Here we describe the development of a plasmid-
561 based transfection method for efficient production and release of SARS-CoV VLPs
562 in permissive Vero E6 green monkey kidney epithelial cells. In contrast to reports
563 on other coronaviruses, we demonstrate that all three M, E and N SARS-CoV
564 structural proteins are required for efficient assembly and release of VLPs by
565 transfected cells. When the S viral envelope glycoprotein is co-expressed with M,
566 N and E, trimers of S are incorporated onto VLPs. Of particular interest is the
567 finding that incorporation of a fluorescently tagged N protein into VLPs allows
568 visualization of transport of *de-novo* formed particles in producer cells. Fluorescent
569 VLPs constitute a new powerful model to study the mechanisms of SARS-CoV
570 egress in living cells and specific roles of cellular machineries by fluorescence
571 imaging techniques.

572 Other research groups have described formation of SARS-CoV VLPs in either
573 insect (26, 44, 50) or mammalian cells (27-29), using various expression systems.

574 Huang Y. and colleagues were the first to report generation of SARS-CoV VLPs in
575 human 293 renal epithelial cells (29). Human codon optimized genes encoding for
576 M, E, N and S proteins were subcloned into mammalian expression vector and
577 VLP formation was monitored by transmission electron microscopy on transfected
578 cells at 63 hours post-transfection. The authors show that, in their experimental
579 conditions, M and N are necessary and sufficient for formation of intracellular
580 VLPs, independently of E and S, but secretion of VLPs was not efficient.
581 Moreover, they described S as an important viral factor for maturation and egress

582 of VLPs from cells, but release of M-N-S VLPs in culture medium was still
583 inefficient. By contrast, in our system we detected sedimentable M and N proteins
584 in culture medium from M plus N expressing cells, suggesting that M-N VLPs can
585 form and be secreted (Figure 1). Furthermore, co-expression of E greatly boosted
586 levels of VLPs detected in culture medium (Figure 1) and addition of S did not
587 influence the rate of VLP production (Figure 2 and data not shown). In contrast,
588 Hsieh and colleagues have described that co-expressed E and M proteins are
589 released four days post-transfection in culture medium of Vero E6 cells in the
590 absence of S and N proteins. In their study, Vero E6 cells, previously infected with
591 a recombinant vaccinia virus harboring the T7 polymerase gene, were co-
592 transfected with plasmids encoding MycHis or V5His-tagged S, M, E and N
593 structural proteins. Nevertheless, sedimentable E and M proteins were also found
594 in culture medium even when they were individually expressed and very high
595 amounts of E were found in VLP preparations in comparison to other viral proteins,
596 suggesting formation of E-containing vesicles. Others have described that MHV
597 and IBV E protein expressed alone results in assembly of E-protein-containing
598 vesicles, with a density similar to that of VLPs (7, 47). We too did find
599 sedimentable SARS-CoV E proteins in culture medium from individually pcDNA-E
600 transfected cells, suggesting secretion of E vesicles, but we could not detect them
601 in any fraction after sucrose gradient fractionation, suggesting a low production
602 rate (Figure 1). We could also detect M-E VLPs at 48 hours post-transfection by
603 coexpressing both E and M proteins, albeit at very low levels (Figure 1A, B and C).
604 In our study, we took advantage of the pIRES bicistronic vector to ensure
605 concomitant expression of E and M and maintain a low expression level for E. We
606 show that use of this vector system, in combination with expression of N, ensures

607 slightly better levels of M-E-N VLPs in medium and great incorporation of E
608 (Figure 1B). Higher levels of E were expressed when an individual pcDNA-E
609 vector was used for E expression and resulted in increased E/M and E/N ratio in
610 cell medium (Figure 1B). We could not conclude whether this was due to higher
611 level of E incorporation into VLPs or to simultaneous release of E-containing
612 vesicles and VLPs. Analysis of viral protein in cell medium by sucrose gradient
613 fractionation revealed that E was only released at significant levels when co-
614 expressed with M and N proteins, with which it cosediments (Figure 1C, panels b,
615 c and e). We have observed efficient M-E-N-S VLP formation and release in 293T,
616 HeLa and Huh-7 human cell lines (data not shown). Consistently, formation and
617 release of M-E-N-S VLPs from 293T cells has been shown in another study
618 reported by Huang C. and colleagues, in which authors have used a pCAGGS
619 mammalian expression plasmid-based transfection system (28). Huang C. and
620 colleagues were able to generate approximately 1.3 μg of SARS-CoV VLPs from
621 $2 \cdot 10^7$ 293T cells (42). Recently, we have measured quantity of S incorporated into
622 envelope of M-E-N-S VLPs purified from the VLP-containing sucrose fractions in
623 our system. Approximately 1 μg and 28 μg of S were present in VLP preparations
624 from 10^7 VeroE6 and 293T cells, respectively (data not shown).

625 We also investigated formation and secretion of SARS-CoV VLPs in transfected
626 cells by transmission electron microscopy and negative staining of purified
627 secreted particles (Figure 3). We were able to identify budding events in
628 cytoplasmic perinuclear compartments. VLP-containing vesicles were scattered
629 within the cytoplasm and found beneath the plasma membrane. Occasionally,
630 secreted VLPs were bound to the cell surface. The VLPs-associated
631 compartments that we observed in transfected Vero E6 cells share significant

632 similarities with the virions-containing compartments described in SARS-CoV
633 infected Vero E6 cells at 3-5 days post infection (23). VLPs were readily detected
634 in sedimented fractions from culture medium by negative staining and electron
635 microscopy (Figure 3H). Globular structures protruding from VLP envelope, and
636 which should correspond to spike peplomers, were occasionally detected, but we
637 could not identify any particle displaying a typical corona-like structure attesting for
638 optimal incorporation of spike trimers on virion envelope.

639 Interestingly, we found that a C-terminal Flag or eYFP tag affects levels of S
640 trimers incorporation onto VLPs (data not shown and Figure 5, respectively).
641 However Sflag and SeYFP proteins could still be incorporated into VLPs and tags
642 can be used as markers. Similar results had been obtained for MHV where S
643 sequence had been extended by fusion with a GFP fluorescent protein (3). These
644 data can be explained by several factors: the 30 KDa fluorescent protein may
645 cause geometrical constraints; M-S interactions, which are important for S
646 incorporation may be affected by the tag; S retention to the site of viral assembly
647 may be disturbed (43, 48). We also tried to produce VLPs containing the mRFP1
648 fluorescent protein fused to the C-terminal end of M (Figure 4 and 5A). Although
649 MmRFP1 was expressed in transfected cells, production of VLPs was abrogated.
650 The M endodomain is crucial for M-N, M-E and M-S interactions and VLP
651 formation (8, 11, 13, 19) and its fusion to a fluorescent protein tag may affect its
652 structure and/or availability for interaction with other partners. This hypothesis is
653 reinforced by the complete loss of recognition of the chimeric MmRFP1 by a rabbit
654 serum raised against a C-terminal peptide of M (Figure 5A, left panel).

655 Lastly, a fusion NeCFP protein could be expressed and assemble into VLPs with
656 M, E and S, although levels of VLPs detected in culture medium were significantly

657 reduced (Figure 5). Interestingly, whereas individually expressed NeCFP or
658 NeGFP were found in the cell cytosol, often accumulating in the perinuclear area,
659 the tagged N protein had a tendency to display a vesicular distribution pattern
660 when co-expressed with M and E (Figure 6). We analyzed both distribution and
661 trafficking of the NeGFP protein in transfected live cells by confocal microscopy
662 (Figure 6B). When cells were co-transfected with pIRES-M-E and pcDNA-NeGFP,
663 the NeGFP proteins were often found in static compartment near the nucleus, in
664 trafficking vesicles scattered in the cytosol and moving actively, making transient
665 interactions with other vesicles, and as small dot scattered at the cortical area
666 beneath the plasma membrane, often enriched in cell projections. Fluorescent
667 dots were also detected in the cell medium surrounding living cells. Subcellular
668 distribution of NeGFP is consistent with our data of transmission electron
669 microscopy. Most likely perinuclear static compartments and trafficking vesicles
670 identified by fluorescence microscopy correspond to perinuclear vacuoles, at
671 which membranes VLP budding events were observed, and to VLP-containing
672 vesicles found by electron microscopy, respectively. The fluorescent dots
673 observed at the cell cortical area may correspond to smaller secretory vesicles
674 containing fewer VLPs – vesicles containing only one VLP were found by electron
675 microscopy – and/or to released VLPs, which are bound to the cell surface.
676 Interestingly, transport of fluorescent vesicles was affected by the drug BFA, well
677 known to affect membrane transport in the secretory pathway (39, 59). BFA
678 treatment induced backward trafficking of fluorescent vesicles and fusion into
679 bright perinuclear clusters (Figure 6C panels a, b and c). Long lasting BFA
680 treatment resulted in suppression of vesicle trafficking and no fluorescent puncta

681 were found at plasma membrane (Figure 6C panel g) and recovery of vesicle
682 trafficking was restored after several hours in normal medium (Figure 6C panel i).
683 Altogether, our data demonstrate that M, E and N structural proteins are key
684 molecules for assembly and egress of the SARS-CoV. Production and analysis of
685 fluorescent M-E-NeGFP SARS-CoV VLPs in living cells allowed us to identify
686 three subcellular structures with different velocity characteristics along the
687 secretory pathway. Molecular and cellular determinants of SARS-CoV assembly
688 and egress will be investigated further using advanced fluorescence microscopy
689 techniques.

ACCEPTED

Acknowledgements

690

691

692 We would like to thank Dr KH Chan (Department of Microbiology, University of
693 Hong Kong) for the gift of the mouse monoclonal antibody against the SARS-CoV
694 N protein, and Professor Roger Y Tsien (University of California, San Diego) for
695 providing us with the plasmid coding for the mRFP1 protein. Special thanks to the
696 Electron microscope Unit of The University of Hong Kong, Li Ka Shing Faculty of
697 Medicine, to Mme Marie-Christine Prevost and Dr Martin Sachse (Plate-Forme de
698 Microscopie Electronique, Institut Pasteur) for their expert advices on electron
699 microscopy experiments; to Ms Iris Ng (Department of Microbiology, University of
700 Hong Kong) for her technical support for electron microscopy experiments; and to
701 Mr Tony Chan (Department of Anatomy, Li Ka Shing Faculty of Medicine Core
702 Imaging Facility, University of Hong Kong) for his technical support during the live
703 cell imaging experiments. KTT is a PhD student supported by the University of
704 Hong Kong. This work was supported by the French Ministry of Health (through
705 the RESPARI Program of the International Network of Institut Pasteur), the French
706 Chancery of Paris Universities and the EU-6th Framework Program (EPISARS).

References

707

708

- 709 1. **Baudoux, P., C. Carrat, L. Besnardeau, B. Charley, and H. Laude.** 1998.
710 Coronavirus pseudoparticles formed with recombinant M and E proteins induce
711 alpha interferon synthesis by leukocytes. *J Virol* **72**:8636-43.
- 712 2. **Bos, E. C., W. Luytjes, H. V. van der Meulen, H. K. Koerten, and W. J.**
713 **Spaan.** 1996. The production of recombinant infectious DI-particles of a murine
714 coronavirus in the absence of helper virus. *Virology* **218**:52-60.
- 715 3. **Bosch, B. J., C. A. de Haan, and P. J. Rottier.** 2004. Coronavirus spike
716 glycoprotein, extended at the carboxy terminus with green fluorescent protein, is
717 assembly competent. *J Virol* **78**:7369-78.
- 718 4. **Bosch, B. J., C. A. de Haan, S. L. Smits, and P. J. Rottier.** 2005. Spike
719 protein assembly into the coronavirion: exploring the limits of its sequence
720 requirements. *Virology* **334**:306-18.
- 721 5. **Campbell, R. E., O. Tour, A. E. Palmer, P. A. Steinbach, G. S. Baird, D.**
722 **A. Zacharias, and R. Y. Tsien.** 2002. A monomeric red fluorescent protein. *Proc*
723 *Natl Acad Sci U S A* **99**:7877-82.
- 724 6. **Caul, E. O., and S. I. Egglestone.** 1977. Further studies on human enteric
725 coronaviruses. *Arch Virol* **54**:107-17.
- 726 7. **Corse, E., and C. E. Machamer.** 2000. Infectious bronchitis virus E protein
727 is targeted to the Golgi complex and directs release of virus-like particles. *J Virol*
728 **74**:4319-26.
- 729 8. **Corse, E., and C. E. Machamer.** 2003. The cytoplasmic tails of infectious
730 bronchitis virus E and M proteins mediate their interaction. *Virology* **312**:25-34.

- 731 9. **Curtis, K. M., B. Yount, and R. S. Baric.** 2002. Heterologous gene
732 expression from transmissible gastroenteritis virus replicon particles. *J Virol*
733 **76**:1422-34.
- 734 10. **Dasgupta, A., and D. W. Wilson.** 2001. Evaluation of the primary effect of
735 brefeldin A treatment upon herpes simplex virus assembly. *J Gen Virol* **82**:1561-7.
- 736 11. **de Haan, C. A., L. Kuo, P. S. Masters, H. Vennema, and P. J. Rottier.**
737 1998. Coronavirus particle assembly: primary structure requirements of the
738 membrane protein. *J Virol* **72**:6838-50.
- 739 12. **de Haan, C. A., and P. J. Rottier.** 2005. Molecular interactions in the
740 assembly of coronaviruses. *Adv Virus Res* **64**:165-230.
- 741 13. **de Haan, C. A., M. Smeets, F. Vernooij, H. Vennema, and P. J. Rottier.**
742 1999. Mapping of the coronavirus membrane protein domains involved in
743 interaction with the spike protein. *J Virol* **73**:7441-52.
- 744 14. **de Haan, C. A., H. Vennema, and P. J. Rottier.** 2000. Assembly of the
745 coronavirus envelope: homotypic interactions between the M proteins. *J Virol*
746 **74**:4967-78.
- 747 15. **Decaro, N., V. Mari, C. Desario, M. Campolo, G. Elia, V. Martella, G.**
748 **Greco, F. Cirone, M. L. Colaianni, P. Cordioli, and C. Buonavoglia.** 2008.
749 Severe outbreak of bovine coronavirus infection in dairy cattle during the warmer
750 season. *Vet Microbiol* **126**:30-9.
- 751 16. **DeDiego, M. L., E. Alvarez, F. Almazan, M. T. Rejas, E. Lamirande, A.**
752 **Roberts, W. J. Shieh, S. R. Zaki, K. Subbarao, and L. Enjuanes.** 2007. A
753 severe acute respiratory syndrome coronavirus that lacks the E gene is attenuated
754 in vitro and in vivo. *J Virol* **81**:1701-13.

- 755 17. **Dubois-Dalcq, M. E., E. W. Doller, M. V. Haspel, and K. V. Holmes.**
756 1982. Cell tropism and expression of mouse hepatitis viruses (MHV) in mouse
757 spinal cord cultures. *Virology* **119**:317-31.
- 758 18. **Erles, K., C. Toomey, H. W. Brooks, and J. Brownlie.** 2003. Detection of
759 a group 2 coronavirus in dogs with canine infectious respiratory disease. *Virology*
760 **310**:216-23.
- 761 19. **Escors, D., J. Ortego, H. Laude, and L. Enjuanes.** 2001. The membrane
762 M protein carboxy terminus binds to transmissible gastroenteritis coronavirus core
763 and contributes to core stability. *J Virol* **75**:1312-24.
- 764 20. **Fischer, F., C. F. Stegen, P. S. Masters, and W. A. Samsonoff.** 1998.
765 Analysis of constructed E gene mutants of mouse hepatitis virus confirms a pivotal
766 role for E protein in coronavirus assembly. *J Virol* **72**:7885-94.
- 767 21. **Fouchier, R. A., T. Kuiken, M. Schutten, G. van Amerongen, G. J. van**
768 **Doornum, B. G. van den Hoogen, M. Peiris, W. Lim, K. Stohr, and A. D.**
769 **Osterhaus.** 2003. Aetiology: Koch's postulates fulfilled for SARS virus. *Nature*
770 **423**:240.
- 771 22. **Godet, M., R. L'Haridon, J. F. Vautherot, and H. Laude.** 1992. TGEV
772 corona virus ORF4 encodes a membrane protein that is incorporated into virions.
773 *Virology* **188**:666-75.
- 774 23. **Goldsmith, C. S., K. M. Tatti, T. G. Ksiazek, P. E. Rollin, J. A. Comer, W.**
775 **W. Lee, P. A. Rota, B. Bankamp, W. J. Bellini, and S. R. Zaki.** 2004.
776 Ultrastructural characterization of SARS coronavirus. *Emerg Infect Dis* **10**:320-6.
- 777 24. **He, R., F. Dobie, M. Ballantine, A. Leeson, Y. Li, N. Bastien, T. Cutts, A.**
778 **Andonov, J. Cao, T. F. Booth, F. A. Plummer, S. Tyler, L. Baker, and X. Li.**

779 2004. Analysis of multimerization of the SARS coronavirus nucleocapsid protein.
780 *Biochem Biophys Res Commun* **316**:476-83.

781 25. **He, R., A. Leeson, M. Ballantine, A. Andonov, L. Baker, F. Dobie, Y. Li,**
782 **N. Bastien, H. Feldmann, U. Strocher, S. Theriault, T. Cutts, J. Cao, T. F.**
783 **Booth, F. A. Plummer, S. Tyler, and X. Li.** 2004. Characterization of protein-
784 protein interactions between the nucleocapsid protein and membrane protein of
785 the SARS coronavirus. *Virus Res* **105**:121-5.

786 26. **Ho, Y., P. H. Lin, C. Y. Liu, S. P. Lee, and Y. C. Chao.** 2004. Assembly of
787 human severe acute respiratory syndrome coronavirus-like particles. *Biochem*
788 *Biophys Res Commun* **318**:833-8.

789 27. **Hsieh, P. K., S. C. Chang, C. C. Huang, T. T. Lee, C. W. Hsiao, Y. H.**
790 **Kou, I. Y. Chen, C. K. Chang, T. H. Huang, and M. F. Chang.** 2005. Assembly of
791 severe acute respiratory syndrome coronavirus RNA packaging signal into virus-
792 like particles is nucleocapsid dependent. *J Virol* **79**:13848-55.

793 28. **Huang, C., N. Ito, C. T. Tseng, and S. Makino.** 2006. Severe acute
794 respiratory syndrome coronavirus 7a accessory protein is a viral structural protein.
795 *J Virol* **80**:7287-94.

796 29. **Huang, Y., Z. Y. Yang, W. P. Kong, and G. J. Nabel.** 2004. Generation of
797 synthetic severe acute respiratory syndrome coronavirus pseudoparticles:
798 implications for assembly and vaccine production. *J Virol* **78**:12557-65.

799 30. **Hurst, K. R., L. Kuo, C. A. Koetzner, R. Ye, B. Hsue, and P. S. Masters.**
800 2005. A major determinant for membrane protein interaction localizes to the
801 carboxy-terminal domain of the mouse coronavirus nucleocapsid protein. *J Virol*
802 **79**:13285-97.

- 803 31. **Kam, Y. W., F. Kien, A. Roberts, Y. C. Cheung, E. W. Lamirande, L.**
804 **Vogel, S. L. Chu, J. Tse, J. Guarner, S. Zaki, K. Subbarao, M. Peiris, B. Nal,**
805 **and R. Altmeyer.** 2006. Antibodies against trimeric S glycoprotein protect
806 hamsters against SARS-CoV challenge despite their capacity to mediate
807 FcγRII-dependent entry into B cells in vitro. *Vaccine*.
- 808 32. **Klumperman, J., J. K. Locker, A. Meijer, M. C. Horzinek, H. J. Geuze,**
809 **and P. J. Rottier.** 1994. Coronavirus M proteins accumulate in the Golgi complex
810 beyond the site of virion budding. *J Virol* **68**:6523-34.
- 811 33. **Krijnse-Locker, J., M. Ericsson, P. J. Rottier, and G. Griffiths.** 1994.
812 Characterization of the budding compartment of mouse hepatitis virus: evidence
813 that transport from the RER to the Golgi complex requires only one vesicular
814 transport step. *J Cell Biol* **124**:55-70.
- 815 34. **Ksiazek, T. G., D. Erdman, C. S. Goldsmith, S. R. Zaki, T. Peret, S.**
816 **Emery, S. Tong, C. Urbani, J. A. Comer, W. Lim, P. E. Rollin, S. F. Dowell, A.**
817 **E. Ling, C. D. Humphrey, W. J. Shieh, J. Guarner, C. D. Paddock, P. Rota, B.**
818 **Fields, J. DeRisi, J. Y. Yang, N. Cox, J. M. Hughes, J. W. LeDuc, W. J. Bellini,**
819 **and L. J. Anderson.** 2003. A novel coronavirus associated with severe acute
820 respiratory syndrome. *N Engl J Med* **348**:1953-66.
- 821 35. **Kuo, L., K. R. Hurst, and P. S. Masters.** 2007. Exceptional flexibility in the
822 sequence requirements for coronavirus small envelope protein function. *J Virol*
823 **81**:2249-62.
- 824 36. **Kuo, L., and P. S. Masters.** 2002. Genetic evidence for a structural
825 interaction between the carboxy termini of the membrane and nucleocapsid
826 proteins of mouse hepatitis virus. *J Virol* **76**:4987-99.

- 827 37. **Kuo, L., and P. S. Masters.** 2003. The small envelope protein E is not
828 essential for murine coronavirus replication. *J Virol* **77**:4597-608.
- 829 38. **Lim, K. P., and D. X. Liu.** 2001. The missing link in coronavirus assembly.
830 Retention of the avian coronavirus infectious bronchitis virus envelope protein in
831 the pre-Golgi compartments and physical interaction between the envelope and
832 membrane proteins. *J Biol Chem* **276**:17515-23.
- 833 39. **Lippincott-Schwartz, J., L. C. Yuan, J. S. Bonifacino, and R. D.**
834 **Klausner.** 1989. Rapid redistribution of Golgi proteins into the ER in cells treated
835 with brefeldin A: evidence for membrane cycling from Golgi to ER. *Cell* **56**:801-13.
- 836 40. **Liu, D. X., and S. C. Inglis.** 1991. Association of the infectious bronchitis
837 virus 3c protein with the virion envelope. *Virology* **185**:911-7.
- 838 41. **Locker, J. K., D. J. Opstelten, M. Ericsson, M. C. Horzinek, and P. J.**
839 **Rottier.** 1995. Oligomerization of a trans-Golgi/trans-Golgi network retained
840 protein occurs in the Golgi complex and may be part of its retention. *J Biol Chem*
841 **270**:8815-21.
- 842 42. **Lokugamage, K. G., N. Yoshikawa-Iwata, N. Ito, D. M. Watts, P. R.**
843 **Wyde, N. Wang, P. Newman, C. T. Kent Tseng, C. J. Peters, and S. Makino.**
844 2008. Chimeric coronavirus-like particles carrying severe acute respiratory
845 syndrome coronavirus (SCoV) S protein protect mice against challenge with
846 SCoV. *Vaccine* **26**:797-808.
- 847 43. **Lontok, E., E. Corse, and C. E. Machamer.** 2004. Intracellular Targeting
848 Signals Contribute to Localization of Coronavirus Spike Proteins near the Virus
849 Assembly Site. *J Virol* **78**:5913-22.
- 850 44. **Lu, X., Y. Chen, B. Bai, H. Hu, L. Tao, J. Yang, J. Chen, Z. Chen, Z. Hu,**
851 **and H. Wang.** 2007. Immune responses against severe acute respiratory

852 syndrome coronavirus induced by virus-like particles in mice. Immunology
853 **122**:496-502.

854 45. **Luo, H., D. Wu, C. Shen, K. Chen, X. Shen, and H. Jiang.** 2006. Severe
855 acute respiratory syndrome coronavirus membrane protein interacts with
856 nucleocapsid protein mostly through their carboxyl termini by electrostatic
857 attraction. *Int J Biochem Cell Biol* **38**:589-99.

858 46. **Madan, V., J. Garcia Mde, M. A. Sanz, and L. Carrasco.** 2005. Viroporin
859 activity of murine hepatitis virus E protein. *FEBS Lett* **579**:3607-12.

860 47. **Maeda, J., A. Maeda, and S. Makino.** 1999. Release of coronavirus E
861 protein in membrane vesicles from virus-infected cells and E protein-expressing
862 cells. *Virology* **263**:265-72.

863 48. **McBride, C. E., J. Li, and C. E. Machamer.** 2007. The cytoplasmic tail of
864 the severe acute respiratory syndrome coronavirus spike protein contains a novel
865 endoplasmic reticulum retrieval signal that binds COPI and promotes interaction
866 with membrane protein. *J Virol* **81**:2418-28.

867 49. **Mirazimi, A., C. H. von Bonsdorff, and L. Svensson.** 1996. Effect of
868 brefeldin A on rotavirus assembly and oligosaccharide processing. *Virology*
869 **217**:554-63.

870 50. **Mortola, E., and P. Roy.** 2004. Efficient assembly and release of SARS
871 coronavirus-like particles by a heterologous expression system. *FEBS Lett*
872 **576**:174-8.

873 51. **Nal, B., C. Chan, F. Kien, L. Siu, J. Tse, K. Chu, J. Kam, I. Staropoli, B.**
874 **Crescenzo-Chaigne, N. Escriou, S. van der Werf, K. Y. Yuen, and R.**
875 **Altmeyer.** 2005. Differential maturation and subcellular localization of severe

- 876 acute respiratory syndrome coronavirus surface proteins S, M and E. *J Gen Virol*
877 **86**:1423-34.
- 878 52. **Narayanan, K., K. H. Kim, and S. Makino.** 2003. Characterization of N
879 protein self-association in coronavirus ribonucleoprotein complexes. *Virus Res*
880 **98**:131-40.
- 881 53. **Narayanan, K., A. Maeda, J. Maeda, and S. Makino.** 2000.
882 Characterization of the coronavirus M protein and nucleocapsid interaction in
883 infected cells. *J Virol* **74**:8127-34.
- 884 54. **Narayanan, K., and S. Makino.** 2001. Characterization of nucleocapsid-M
885 protein interaction in murine coronavirus. *Adv Exp Med Biol* **494**:577-82.
- 886 55. **Nguyen, V. P., and B. G. Hogue.** 1997. Protein interactions during
887 coronavirus assembly. *J Virol* **71**:9278-84.
- 888 56. **Nicholls, J. M., J. Butany, L. L. Poon, K. H. Chan, S. L. Beh, S.**
889 **Poutanen, J. S. Peiris, and M. Wong.** 2006. Time course and cellular localization
890 of SARS-CoV nucleoprotein and RNA in lungs from fatal cases of SARS. *PLoS*
891 *Med* **3**:e27.
- 892 57. **Ortego, J., D. Escors, H. Laude, and L. Enjuanes.** 2002. Generation of a
893 replication-competent, propagation-deficient virus vector based on the
894 transmissible gastroenteritis coronavirus genome. *J Virol* **76**:11518-29.
- 895 58. **Peiris, J. S., S. T. Lai, L. L. Poon, Y. Guan, L. Y. Yam, W. Lim, J.**
896 **Nicholls, W. K. Yee, W. W. Yan, M. T. Cheung, V. C. Cheng, K. H. Chan, D. N.**
897 **Tsang, R. W. Yung, T. K. Ng, and K. Y. Yuen.** 2003. Coronavirus as a possible
898 cause of severe acute respiratory syndrome. *Lancet* **361**:1319-25.
- 899 59. **Pelham, H. R.** 1991. Multiple targets for brefeldin A. *Cell* **67**:449-51.

- 900 60. **Rota, P. A., M. S. Oberste, S. S. Monroe, W. A. Nix, R. Campagnoli, J. P.**
901 **Icenogle, S. Penaranda, B. Bankamp, K. Maher, M. H. Chen, S. Tong, A.**
902 **Tamin, L. Lowe, M. Frace, J. L. DeRisi, Q. Chen, D. Wang, D. D. Erdman, T. C.**
903 **Peret, C. Burns, T. G. Ksiazek, P. E. Rollin, A. Sanchez, S. Liffick, B.**
904 **Holloway, J. Limor, K. McCaustland, M. Olsen-Rasmussen, R. Fouchier, S.**
905 **Gunther, A. D. Osterhaus, C. Drosten, M. A. Pallansch, L. J. Anderson, and**
906 **W. J. Bellini.** 2003. Characterization of a novel coronavirus associated with
907 severe acute respiratory syndrome. *Science* **300**:1394-9.
- 908 61. **Schelle, B., N. Karl, B. Ludewig, S. G. Siddell, and V. Thiel.** 2006.
909 Nucleocapsid protein expression facilitates coronavirus replication. *Adv Exp Med*
910 *Biol* **581**:43-8.
- 911 62. **Stertz, S., M. Reichelt, M. Spiegel, T. Kuri, L. Martinez-Sobrido, A.**
912 **Garcia-Sastre, F. Weber, and G. Kochs.** 2007. The intracellular sites of early
913 replication and budding of SARS-coronavirus. *Virology* **361**:304-15.
- 914 63. **Tooze, J., S. Tooze, and G. Warren.** 1984. Replication of coronavirus
915 MHV-A59 in sac- cells: determination of the first site of budding of progeny virions.
916 *Eur J Cell Biol* **33**:281-93.
- 917 64. **van der Hoek, L., K. Pyrc, M. F. Jebbink, W. Vermeulen-Oost, R. J.**
918 **Berkhout, K. C. Wolthers, P. M. Wertheim-van Dillen, J. Kaandorp, J.**
919 **Spaargaren, and B. Berkhout.** 2004. Identification of a new human coronavirus.
920 *Nat Med* **10**:368-73.
- 921 65. **Vennema, H., G. J. Godeke, J. W. Rossen, W. F. Voorhout, M. C.**
922 **Horzinek, D. J. Opstelten, and P. J. Rottier.** 1996. Nucleocapsid-independent
923 assembly of coronavirus-like particles by co-expression of viral envelope protein
924 genes. *Embo J* **15**:2020-8.

- 925 66. **Wilson, L., P. Gage, and G. Ewart.** 2006. Hexamethylene amiloride blocks
926 E protein ion channels and inhibits coronavirus replication. *Virology* **353**:294-306.
- 927 67. **Wilson, L., C. McKinlay, P. Gage, and G. Ewart.** 2004. SARS coronavirus
928 E protein forms cation-selective ion channels. *Virology* **330**:322-31.
- 929 68. **Woo, P. C., S. K. Lau, C. M. Chu, K. H. Chan, H. W. Tsoi, Y. Huang, B.**
930 **H. Wong, R. W. Poon, J. J. Cai, W. K. Luk, L. L. Poon, S. S. Wong, Y. Guan, J.**
931 **S. Peiris, and K. Y. Yuen.** 2005. Characterization and complete genome
932 sequence of a novel coronavirus, coronavirus HKU1, from patients with
933 pneumonia. *J Virol* **79**:884-95.
- 934 69. **Woo, P. C., S. K. Lau, K. S. Li, R. W. Poon, B. H. Wong, H. W. Tsoi, B.**
935 **C. Yip, Y. Huang, K. H. Chan, and K. Y. Yuen.** 2006. Molecular diversity of
936 coronaviruses in bats. *Virology* **351**:180-7.
- 937 70. **Ye, Y., and B. G. Hogue.** 2007. Role of the coronavirus E viroporin protein
938 transmembrane domain in virus assembly. *J Virol* **81**:3597-607.
- 939

940 **Figure legends**

941

942 **Figure 1. Production of SARS-CoV VLPs by transfected Vero E6 cells. A.**

943 Coexpression of M, E and N is necessary for efficient secretion of SARS-CoV
944 VLPs by Vero E6 cells at 24 and 48 hours post-transfection. Monolayers of Vero
945 E6 cells were transfected with plasmids driving the expression of SARS-CoV
946 structural proteins M, E and Flag-tagged N as specified on top of each lane.
947 Protein expression in cell lysates and in VLPs isolated from culture medium was
948 analyzed by Western blot at 24 and 48 hours post-transfection, as indicated below
949 corresponding panels. Samples were heat-denatured and reduced with
950 dithiothreitol before loading. The M and E proteins were detected with rabbit
951 polyclonal antibodies produced against the C-terminal extremity of each proteins.
952 The N protein was detected with the M2 monoclonal antibody recognizing the Flag
953 tag. Blots were exposed for 1 minute for signal detection except for detection of E
954 contained in pellets from ultracentrifuged culture medium (bottom panels), for
955 which blots were exposed for 10 minutes. The molecular mass (in kDa) and
956 migration of protein standards are shown between blots. **B.** Use of the bicistronic
957 pIRES-M-E vector restrains E expression level and favors production of M-E-N
958 VLPs. Vero E6 were transfected with indicated plasmid combinations and cell
959 lysates and medium were analyzed at 48 hours post-transfection as in A. To
960 ensure better detection of E, VLPs were concentrated four times more than in A.
961 Blots were exposed for 10 seconds for signal detection except for detection of E
962 contained in pellets from ultracentrifuged culture medium (right bottom panel) for
963 which the blot was exposed for 1 minute. **C.** Secreted viral structural proteins
964 cosediment in sucrose gradient. Three 75 cm² dishes of Vero E6 cells were

965 transfected with plasmids driving the expression of SARS-CoV structural proteins
966 M, E and Flag-tagged N either individually or in combination. Protein expression in
967 cell lysates and in pellets from culture medium ultracentrifuged on 20% sucrose
968 cushion was controlled by Western blot at 48 hours post-transfection (left panel).
969 Resuspended pellets from ultracentrifuged cell medium were then loaded on a 20-
970 60% discontinuous sucrose gradient and subjected to fractionation by
971 ultracentrifugation. Twenty fractions of 600 μ l were collected (1-20, lightest to
972 heaviest). Nature of viral proteins associated with each fraction was determined by
973 Western blot (right panels, a to e). 15 μ l of samples were heat-denatured and
974 reduced with dithiothreitol before loading. The molecular mass (in kDa) and
975 migration of protein standards are shown on the right side of the blots. Samples
976 from pIRES-M, pIRES-E plus pCDNA-E, pIRES-E plus pCDNA-E plus pCDNA-
977 Nflag and pCDNA-E, pIRES-M plus pCDNA-Nflag have been generated in two
978 separate experiments.
979 Ctrl: non-transfected cells; E: pCDNA-E; M: pIRES-M; M-E: pIRES-M-E; M +
980 Nflag: pIRES-M plus pCDNA-Nflag; M-E + Nflag: pIRES-M-E plus pCDNA-Nflag; M
981 + E: pIRES-M + pCDNA-E; M + E + Nflag: pIRES-M plus pCDNA-E plus pCDNA-
982 Nflag.

983

984 **Figure 2. S glycoprotein trimers are incorporated onto SARS-CoV M, E and**
985 **N-containing VLPs.** pCDNA-S plasmid was co-transfected with pIRES-M-E and
986 pCDNA-Nflag vectors. Culture medium was harvested at 48 hours post-
987 transfection, ultracentrifuged on 20% sucrose cushion and pellets were
988 resuspended in TNE buffer and ultracentrifuged on a 20-60% discontinuous
989 sucrose gradient. Twenty fractions were collected (1-20, lightest to heaviest) and

990 analyzed by Western blot. Samples were either heat-denatured and reduced with
991 dithiothreitol before loading for detection of Nflag, M and E or not heated and not
992 reduced for analysis of S. Blots were exposed for 10 seconds for signal detection,
993 except for E for which blots were exposed for 10 minutes. The highest levels of S,
994 M, N and E structural proteins were found in fractions 9 and 10 corresponding to
995 40% sucrose. S protein was detected with mouse polyclonal antibodies raised
996 against purified S trimers. Arrows indicate bands that correspond to trimeric and
997 monomeric forms of S. The molecular mass (in kDa) and migration of protein
998 standards are shown on the right side of the blots.

999

1000 **Figure 3. Structural analysis and intracellular distribution of SARS-CoV**
1001 **VLPs.** Vero E6 cells were co-transfected with pIRES-M-E, pcDNA-Nflag and
1002 pcDNA-S. At 24 and 48 hours post-transfection cells were fixed and ultrathin
1003 sections were analyzed by electron microscopy (panels A to G). **A.** VLPs were
1004 found in intracellular vacuoles (vc), in vesicles (vs) scattered in the cytosol and
1005 bound to the plasma membrane (pm). The arrow points VLPs attached to the cell
1006 surface. **B.** Large amount of VLPs within the lumen of the endoplasmic reticulum
1007 (er) and within a cytoplasmic vesicle. n: nucleus. **C.** Presence of VLPs within
1008 vacuoles and vesicles. Arrows point to small VLPs-containing vesicles beneath the
1009 plasma membrane. **D.** Magnification of a VLP-containing vacuole. Black arrows
1010 point to budding events. **E.** Compacted VLP-containing vesicles were found
1011 beneath the plasma membrane. **F.** VLPs bound to the surface of a producer cell.
1012 Two membrane-bound VLPs are shown by arrows. **G.** VLPs bound to a cell
1013 filopodia. Spike-like protuberances were visible on VLP surface (arrows). **H.**
1014 Electron microscopy images of negatively stained VLPs purified from cell medium

1015 at 48 hours post-transfection. A scale bar is indicated for each picture. A-D and F-
1016 G panels correspond to cells fixed at 48 hours post-transfection. Image E was
1017 taken from cells fixed 24 hours post-transfection. n: nucleus, er: endoplasmic
1018 reticulum, vc: vacuole, vs: vesicle, pm: plasma membrane.

1019

1020 **Figure 4. Expression and subcellular distribution of viral structural proteins**
1021 **tagged with fluorescent proteins.** Vero E6 cells grown on glass coverslips were
1022 either transfected with single plasmids (left panels) or co-transfected (right panels)
1023 with the three plasmids encoding the MmRFP1, E, SeYFP and NeCFP proteins. At
1024 24 hours post-transfection, cells were processed for nuclear staining with DAPI
1025 dye, fixed and analyzed under a fluorescent microscope equipped with an
1026 ApoTome device to acquire images of optical sections. a, b, g, h: MmRFP1; c, d, i,
1027 j: SeYFP; e, f, k, l: NeCFP; m, n: merged images. For all conditions, two
1028 representative images are shown side-by-side.

1029

1030 **Figure 5. Production of fluorescent VLPs by transfected Vero E6 cells. A.**
1031 Determination of optimal plasmid combinations for production of SARS-CoV
1032 fluorescent VLPs. Viral proteins from cell lysates (left panel) and sedimented VLPs
1033 from medium (right panel) were analyzed by Western blot. VLPs could be
1034 produced when either N or S (lanes 9 and 10) but not M (lane 8) were tagged with
1035 fluorescent proteins. **B.** Production of fluorescent VLPs and efficiency of
1036 incorporation of NeCFP and SeYFP fusion proteins into VLPs. Cells were co-
1037 transfected with the specified plasmid combinations (corresponding to lanes 9 and
1038 10 of panel A) and purified VLPs from medium were analyzed by sucrose gradient.
1039 Tagging S (lower blot) resulted in a greater yield of VLP production when

1040 compared to tagged N (upper blot). However, the eYFP tag greatly reduced S
1041 incorporation onto VLPs (lower blot). Arrows indicates spike trimers and
1042 monomers.

1043

1044 **Figure 6. Tracking of fluorescent SARS-CoV VLPs in living cells. A.** Widefield
1045 fluorescence microscopy images showing accumulation of fluorescent VLPs at the
1046 plasma membrane of pIRES-M-E plus pcDNA-NeCFP co-transfected cells (panels
1047 b), whereas a strong perinuclear staining was observed in Vero E6 expressing
1048 NeCFP alone (panel a). **B.** Confocal microscopy of living cells expressing M-E-
1049 NeGFP VLPs. Four categories of fluorescent signals were observed: a bright and
1050 static large perinuclear compartment (white encircling lines), smaller and dimmer
1051 actively trafficking vesicles (orange encircling lines), bright dots accumulating at
1052 the cell cortex (yellow encircling lines) and dots in the medium surrounding
1053 transfected cells (yellow dots). Videos are available as Supplemental Material. **C.**
1054 Treatment of transfected cells with brefeldin A (BFA) alters trafficking of
1055 fluorescent vesicles. Vero E6 cells were transfected with pIRES-M-E plus pcDNA-
1056 NeGFP plasmids. Cells were either non-treated (a) or treated with 6 μ g/ml of BFA
1057 for either 4 hours (d) or overnight (g). BFA was then added to non-treated cells
1058 and time-lapse acquisitions were performed. Panels b and c show the same cell
1059 than in panel a but after 25 and 70 minutes incubation with the drug. Alternatively,
1060 BFA was washed out and recovery after BFA treatment was analysed (panels e, f
1061 and h, i). Panels a, b and c, d and e, g and h show same cells at different time
1062 points. Video illustrating panels b, d, f, h and I are provided as supplementary
1063 data.

1064

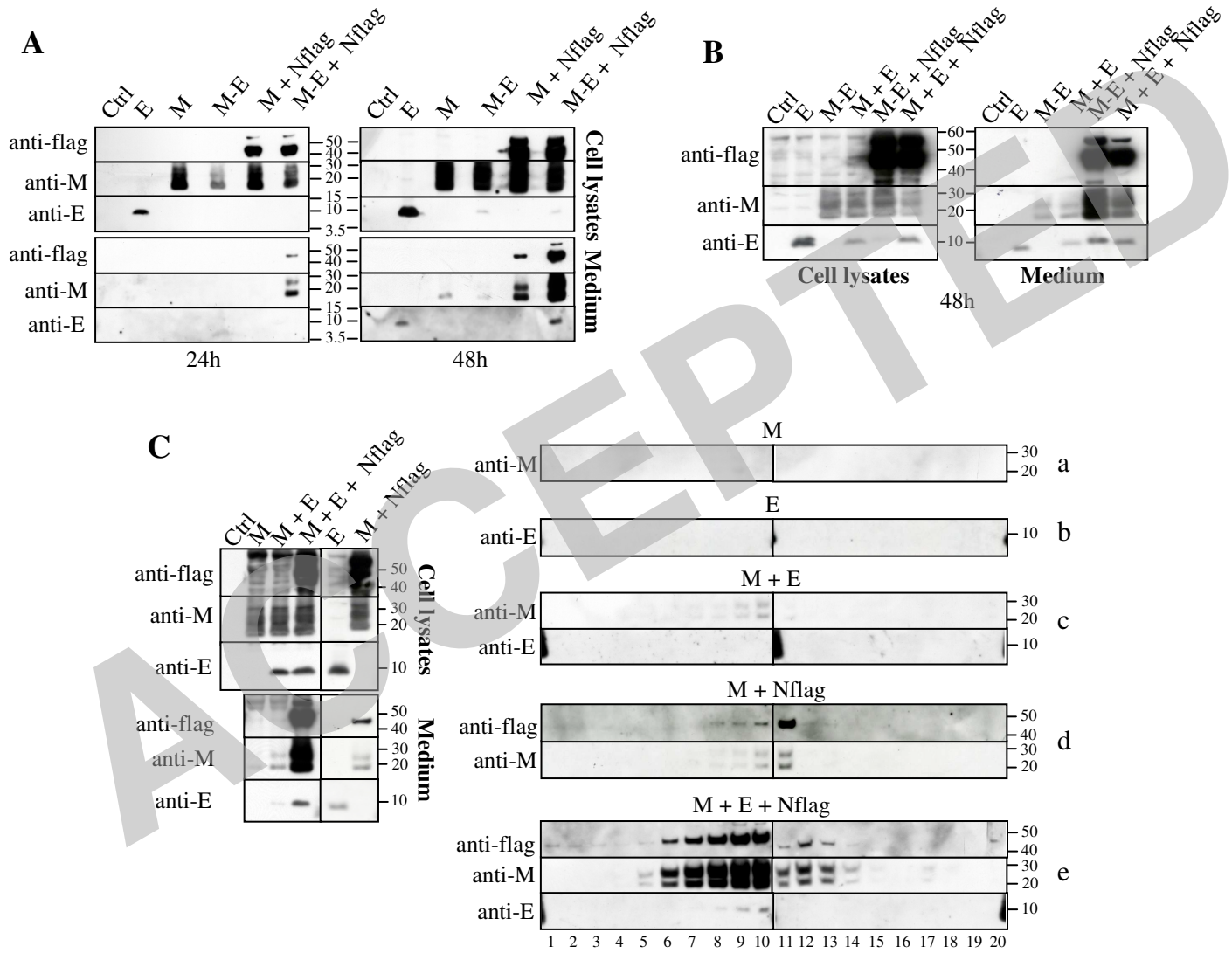


Figure 1

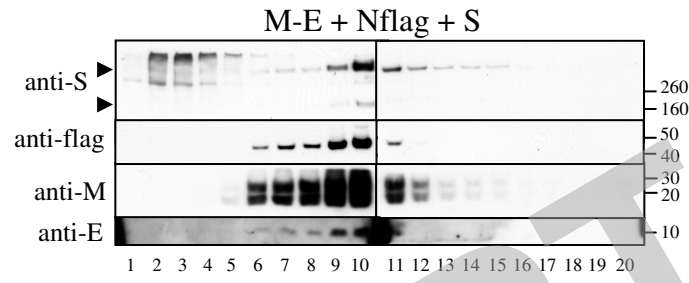


Figure 2

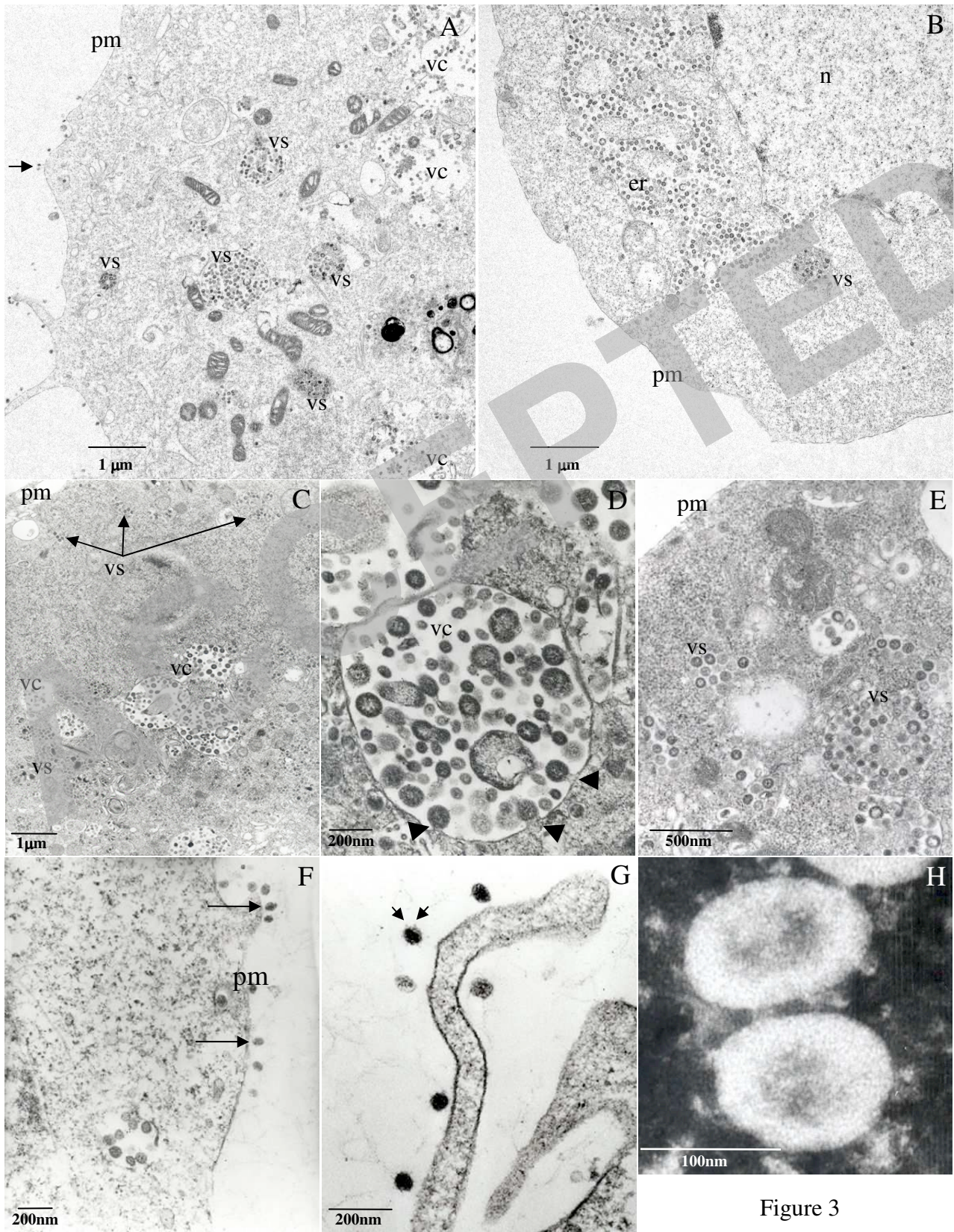


Figure 3

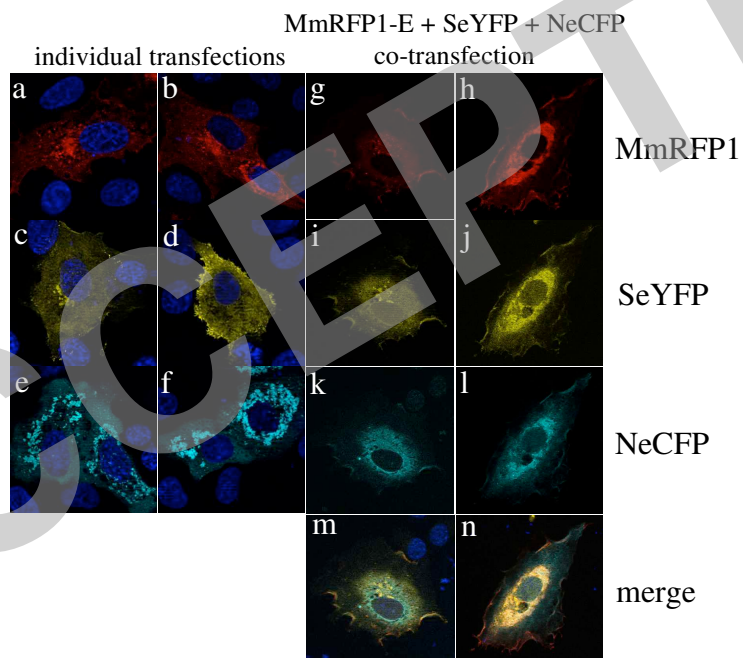


Figure 4

A

	1	2	3	4	5	6	7	8	9	10
M-E	-	+	-	+	+	-	+	-	+	+
MmRFP1-E	-	-	+	-	-	-	-	+	-	-
Nflag	-	+	+	-	+	-	+	+	-	+
NeCFP	-	-	-	+	-	-	-	-	+	-
S	-	+	+	+	-	-	+	+	+	-
SeYFP	-	-	-	-	+	-	-	-	-	+

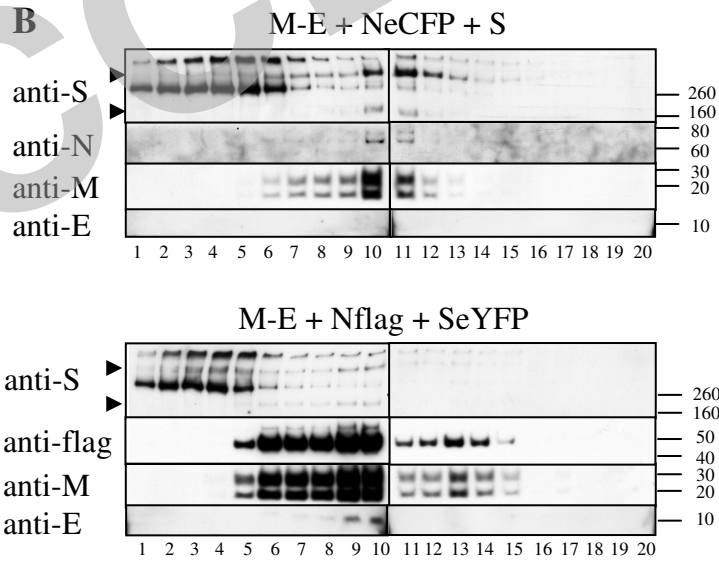
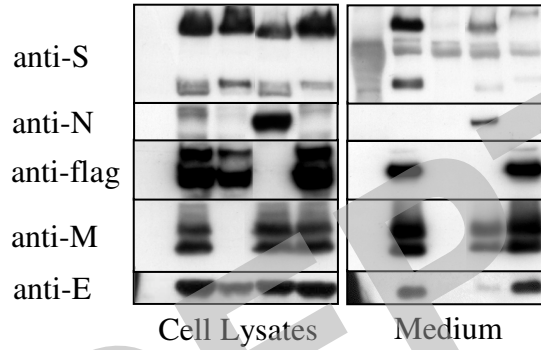


Figure 5

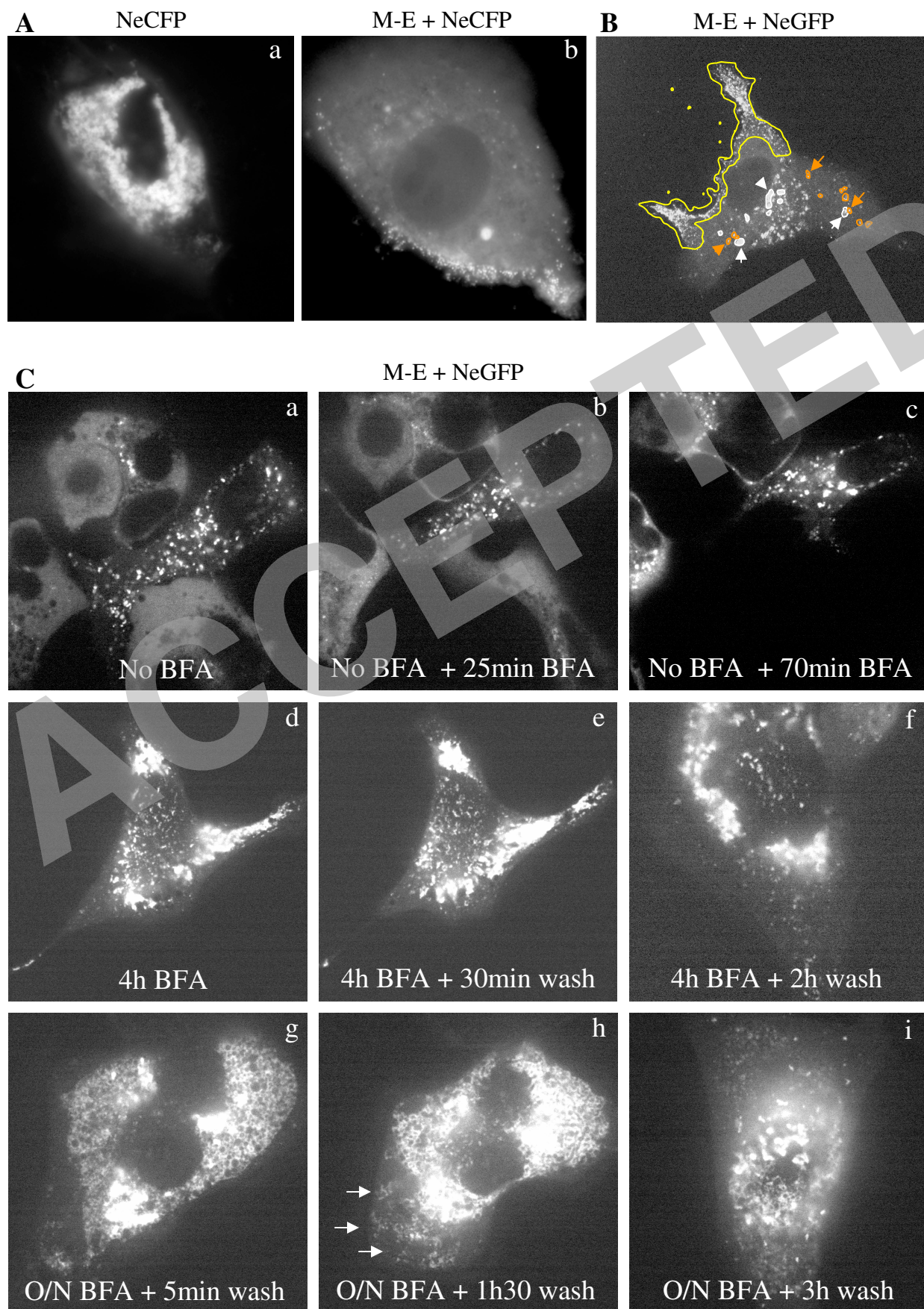


Figure 6